to 2.84 Å. The model has excellent stereochemistry (*44*) (Table 1). The final model (for each QacR-drug complex) includes the drug and residues 2 to 187 of each subunit as well as several sulfate molecules that are associated with residues from the DNA binding domains (Table 1). CNS drug topology and parameter files were obtained using the HIC-Up-server at (http://xray.bmc.uu.se/cgi-bin/gerard/hicup_server.pl). The remaining QacR-drug complexes were prepared and crystallized similarly and their structures are isomorphous with the QacR-R6G structure (Table 1). In each case, the starting QacR model, with drug removed, was subjected to rigid body refinement in CNS followed by SA/positional/thermal parameter refinement. Composite omit maps showing the region around each drug are in Supplementary fig. 3. Relevant intensity data collection, refinement statistics, and resolution limits for all QacR complexes are listed in Table 1. In all QacR-drug complexes Tyr^{92} of the drug-free subunits is a Ramachandran outlier as is, in some cases, Lys^{44} of the DNA binding domain, which has weak density. Figure 2, B to D, and Fig. 3, A to F, were generated with Swiss PDB Viewer (*45*) and rendered with POVRAY (*46*). Figure 4, A and B, was generated using Sybyl6.7. Figure 2A was made with O (*42*).

28. The QacR-R6G equilibrium dialysis experiments were carried out in buffer A [100 mM Hepes (pH 7.5), 250 mM potassium glutamate, 150 mM NaCl, 10 mM MgOAc, 0.5 mM EDTA, and 5% glycerol]. One-milliliter solutions of QacR dimer (400 nM) were dialyzed against 500 ml buffer A containing 75, 110, 150, or 190 nM R6G for 5 days at 4°C with stirring. After dialysis the samples were incubated at 95°C for 5 min (to denature the protein), centrifuged (14,000 rpm for 20 s), and the supernatants measured for R6G fluorescence (λ_{ex} 520 nm, λ_{em} 551 nm). The R6G concentrations in each dialyzed sample and its respective dialysate were quantified by transforming their fluorescence signals with a linear fit to a serial dilution of R6G in buffer A measured in identical fashion. The concentration of "bound" R6G in the QacR containing samples was determined by subtracting the concentration of "free" R6G in a dialyzed blank (Supplementary fig. 2). Control dialysis experiments included the addition of purine repressor (100 nM dimer) or BSA (100 nM) to the QacR solution (as well as their independent testing) and had no effect on QacR-R6G binding affinity.
29. M. Ahmed, C. M. Borsch, S. S. Taylor, N. Vazquez-Laslop, A. A. Neyfakh, *J. Biol. Chem.* **269**, 28506 (1994).
30. A. Brooun, J. J. Tomashek, K. Lewis, *J. Bacteriol.* **181**, 5131 (1999).
31. M. Schumacher *et al.*, unpublished data.
32. P. Orth, D. Schnappinger, W. Hillen, W. Saenger, W. Hinrichs, *Nature Struct. Biol.* **7**, 215 (2000).
33. G. P. Brady Jr., P. F. W. Stouten, *J. Computer-Aided Mol. Des.* **14**, 383 (2000).
34. S. Lovell, B. J. Marquardt, B. Kahr, *J. Chem. Soc. Perkin Trans.* **2**, 2241 (1999).
35. K. Lewis, *J. Mol. Microbiol. Biotechnol.* **3**, 247 (2001).
36. S. Grkovic, M. H. Brown, R. A. Skurray, unpublished data.
37. G. Chang, C. B. Roth, *Science* **293**, 1793 (2001).
38. I. Rayment, *Methods Enzymol.* **276**, 176 (1999).
39. S. Doublié, *Methods Enzymol.* **276**, 523 (1999).
40. T. C. Terwilliger, J. Berendzen, *Acta Crystallogr. D.* **55**, 849 (1999).
41. A. T. Brünger *et al.*, *Acta Crystallogr. D* **54**, 905 (1998).
42. T. A. Jones, J.-T. Zou, S. W. Cowan, M. Kjeldgaard, *Acta Crystallogr. A* **47**, 110 (1991).
43. M. A. Schumacher *et al.*, unpublished data.
44. R. A. Laskowski, M. W. MacArthur, J. M. Thorton, *J. Appl. Crystallogr.* **26**, 283 (1993).
45. N. Guex, M. C. Peitsch, Swiss PDB, *Electrophoresis* **18**, 2714 (1997).
46. POV-Ray, Persistence of Vision Raytracer, version 3.1 (www.povray.org).
47. M.A.S. is a Burroughs Wellcome Career Development Awardee. S.G. was the recipient of an Australian Postgraduate Award. Supported by grants AI 48593 from the NIH to R.G.B. and project grant 153818 from the National Health and Medical Research Council (Australia) to R.A.S. Intensity data collected at the Stanford Synchrotron Radiation Laboratory (SSRL) was carried out under the auspices of the SSRL biotechnology program, which is supported by the NIH, National Center for Research Resources, Biomedical Technology Program, and by the Department of Energy, Office of Biological and Environmental Research. Coordinates and structure factors have been deposited with the Protein Data Bank (Accession codes for the QacR-R6G, QacR-Et, QacR-Dq, QacR-CV, QacR-MG, and QacR-Be complexes are 1JUS, 1JTY, 1JT6, 1JTX, 1JUP, and 1JUM, respectively).

5 September 2001; accepted 26 October 2001

Structural Basis for Selective Recognition of Oligosaccharides by DC-SIGN and DC-SIGNR

Hadar Feinberg,[1] Daniel A. Mitchell,[2] Kurt Drickamer,[2] William I. Weis[1]*

Dendritic cell specific intracellular adhesion molecule–3 (ICAM-3) grabbing nonintegrin (DC-SIGN), a C-type lectin present on the surface of dendritic cells, mediates the initial interaction of dendritic cells with T cells by binding to ICAM-3. DC-SIGN and DC-SIGNR, a related receptor found on the endothelium of liver sinusoids, placental capillaries, and lymph nodes, bind to oligosaccharides that are present on the envelope of human immunodeficiency virus (HIV), an interaction that strongly promotes viral infection of T cells. Crystal structures of carbohydrate-recognition domains of DC-SIGN and of DC-SIGNR bound to oligosaccharide, in combination with binding studies, reveal that these receptors selectively recognize endogenous high-mannose oligosaccharides and may represent a new avenue for developing HIV prophylactics.

Initiation of a primary immune response requires the interaction of resting T cells with antigen-presenting dendritic cells (*1*). Initial interaction of T cells with dendritic cells is mediated by the binding of the T cell surface receptor ICAM-3 to a dendritic cell surface receptor denoted DC-SIGN (*2*). DC-SIGN may also mediate rolling of dendritic cells

Table 1. Data collection and refinement statistics. Unit cell parameters are from postrefinement in SCALEPACK (*20*). Ramachandran plot regions are defined in PROCHECK (*21*).

	DC-SIGN	DC-SIGNR
Space group	C2	$P2_12_12_1$
Unit cell parameters		
a (Å)	106.8	50.2
b (Å)	148.2	57.0
c (Å)	113.0	89.3
β (°)	91.0	
Resolution range (Å)	50 to 2.5 (2.59 to 2.50)	50 to 1.9 (1.97 to 1.90)
Measured reflections	250720	843434
Unique reflections	59357	19033
Completeness (%)	97.8(99.3)	92.0(83.6)
R_{sym}* (%)	5.3(26.6)	7.2(13.1)
R_{cryst}† (%)	21.4	19.4
R_{free}† (%)	25.8	24.0
Rmsd from ideality		
Bonds (Å)	0.0067	0.0049
Angles (°)	1.3	1.2
Ramachandran plot		
% in most favored	87.2	89.0
% in allowed	11.7	10.5
% generous regions	1.1	0.4
% disallowed	0.0	0.0
Average B-factor (Å^2)		
Main chain	47.3	24.0
Side chain	48.7	26.2
Carbohydrate	43.2	35.5
Ca^{2+}	40.8	17.1
Water molecules	41.9	32.6

*$R_{sym} = \Sigma_h\Sigma_i(|I_i(h)| - |\langle I(h)\rangle|)/\Sigma_h\Sigma_i I_i(h)$ where $I_i(h)$ = observed intensity, and $\langle I(h)\rangle$ = mean intensity obtained from multiple measurements. †R_{cryst} and $R_{free} = \Sigma||F_o| - |F_c||/\Sigma|F_o|$, where $|F_o|$ = observed structure factor amplitude and $|F_c|$ = calculated structure factor amplitude for the working and test sets, respectively.

on endothelium through interactions with ICAM-2, as part of the trafficking of dendritic cells from the blood to the lymphatic system (*3*). DC-SIGN is a type II membrane protein in which the extracellular domain consists of a stalk that mediates tetramerization (*4*) and a COOH terminal carbohydrate recognition domain (CRD) that belongs to the C-type (Ca^{2+}-dependent) lectin superfamily (*5*). Activation of T cells by dendritic cells can be inhibited by antibodies to DC-SIGN, Ca^{2+} chelators, mannan, or mannose (*2*), indicating that Ca^{2+}-dependent carbohydrate-binding activity is responsible for the interaction with ICAM-3. DC-SIGNR, a receptor that is 77% identical in sequence to DC-SIGN, is found on liver sinusoidal endothelium and the endothelium of lymph node sinuses and placental villi (*6–8*).

The presence of dendritic cells greatly enhances the efficiency of infection of $CD4^+$ T cells by human and simian immunodeficiency viruses (HIV and SIV) (*9*, *10*). Antibodies to DC-SIGN significantly reduce the level of infection of T cells co-cultured with dendritic cells, and DC-SIGN binds strongly to the HIV envelope glycoprotein gp120, suggesting that this enhancement is mediated by DC-SIGN (*9*). DC-SIGN is abundantly expressed on dendritic cells present in the lamina propria of mucosal tissues such as rectum, uterus, and cervix, leading to the proposal that dendritic cells residing at primary sites of HIV exposure capture the virus and deliver it to T cells in lymphatic tissues (*9*). DC-SIGNR can also bind immunodeficiency virus, suggesting that it may facilitate transmission of HIV across capillaries in the lymph node and at the maternal-fetal boundary (*7*, *8*). Like the dendritic cell–T cell interaction, the interaction of DC-SIGN and DC-SIGNR with HIV is inhibitable by Ca^{2+} chelators and mannan (*7–9*).

In order to determine the precise specificity and mechanism of carbohydrate recognition by these receptors, crystal structures of CRDs from DC-SIGN and DC-SIGNR bound to a pentasaccharide (Fig. 1A) were solved [see also supplemental data (*11*) and Table 1] (Fig. 2A). The DC-SIGNR crystals contain two crystallographically independent molecules, one of which is bound to Ca^{2+} and the pentasaccharide. The DC-SIGN crystals contain pairs of CRDs cross-linked by the oligosaccharide, in which one monomer forms the same contacts with the oligosaccharide observed for DC-SIGNR, while the partner monomer interacts with the terminal *N*-acetylglucosamine (GlcNAc) on the α1-3 branch (GlcNAc1) (Fig. 1A).

The DC-SIGN and DC-SIGNR CRDs adopt the typical long-form C-type lectin fold (*12*) (Fig. 2). The second α helix (α2) (Fig. 2A) is unusually long and lies closer to the rest of the domain than in most C-type lectin-like structures. The COOH-terminal end of the helix packs against the loop connecting β strands 3 and 4, forming a continuous surface that interacts with the bound oligosaccharide (Fig. 2A). In the following text, residue numbers refer to the higher resolution DC-SIGNR structure unless otherwise noted.

The pentasaccharide is exceptionally well defined in both structures [see fig. 1 of supplemental data (*11*)]. Despite the different crystallization conditions and the way that the carbohydrate cross-links two monomeric CRDs in the DC-SIGN crystals, the conformation of the pentasaccharide is identical to within experimental error [see supplemental data (*11*)]. The conformations of the four glycosidic linkages are near their average values found in a survey of crystal structures containing these sugars (*13*) [see table 1 of supplemental data (*11*)]. Thus, both proteins interact with a common, low-energy conformation of the oligosaccharide. The ω angle of the α1-6 linkage lies slightly outside of the normal range for this angle, which may be due to the interaction between this disaccharide moiety (Man3-Man4) and Phe^{325}.

The internal α1-3–linked mannose (Man2) (see Fig. 1A for residue numbering) binds to the Ca^{2+} site found in all C-type lectins. The equatorial 3- and 4-OHs each form coordination bonds with the Ca^{2+} and hydrogen bonds with amino acids that also serve as Ca^{2+} ligands (Fig. 3, A and B). Such interactions with vicinal hydroxyl groups are

[1]Department of Structural Biology and Department of Molecular and Cellular Physiology, Stanford University School of Medicine, Stanford, CA 94305, USA. [2]Glycobiology Institute, Department of Biochemistry, University of Oxford, Oxford OX1 3QU, UK.

*To whom correspondence should be addressed. E-mail: bill.weis@stanford.edu

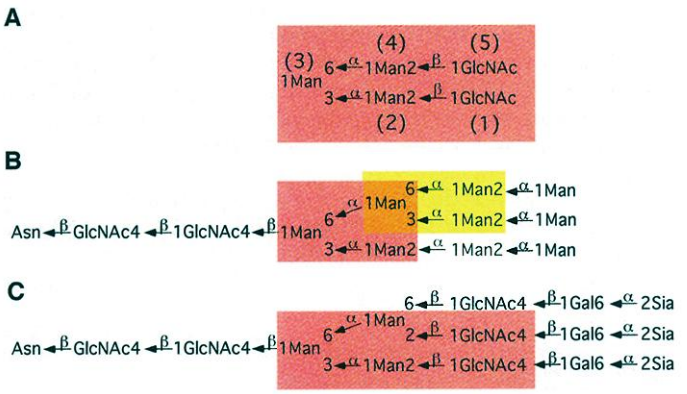

Fig. 1. Oligosaccharide structures. (**A**) The pentasaccharide co-crystallized with both DC-SIGN and DC-SIGNR. Residue numbers used in the text are shown in parentheses. (**B**) N-linked high-mannose structure. The full nine-mannose structure (Man_9) is shown, but the presence of α1-2 linked mannose at the branch termini is variable. The inner branched trimannose structure Manα1-3 [Manα1-6]Man is shown in the red box, and the outer trimannose structure is shown in the yellow box. (**C**) Typical N-linked complex carbohydrate. The portion equivalent to the pentasaccharide used in this study is boxed in red. The inner trimannose structure is common to both complex and high-mannose N-linked oligosaccharides. Gal, galactose; GlcNAc, *N*-acetylglucosamine; Man, mannose; Sia, sialic acid.

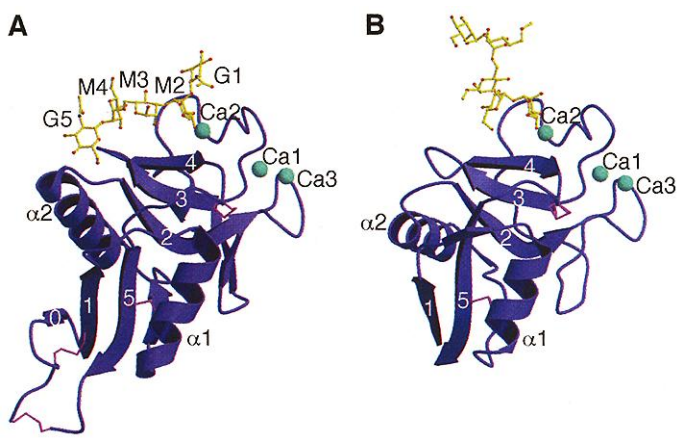

Fig. 2. Structure of the CRD of DC-SIGN bound to $GlcNAc_2Man_3$. (**A**) Ribbon diagram of the DC-SIGN CRD (blue), with the bound oligosaccharide shown in a ball-and-stick representation (yellow-green, bonds and carbon atoms; red, oxygen; blue, nitrogen). Oligosaccharide residues are shown with the single letter code G for GlcNAc and M for mannose. Large cyan spheres are the three Ca^{2+}. Disulfide bonds are shown in pink. The DC-SIGNR complex is very similar, except that the fourth disulfide connecting the NH_2 and COOH termini is not visible in either copy. (**B**) Rat serum mannose-binding protein bound to a high-mannose oligosaccharide (*17*). The color scheme is the same as in (A). A total of 228 $Å^2$ of carbohydrate and 166 $Å^2$ of protein surface area is buried in the MBP-oligosaccharide complex, in contrast to the 445 $Å^2$ of carbohydrate and 328 $Å^2$ of protein surface buried in the DC-SIGNR complex.

hallmarks of C-type lectin-carbohydrate interactions (*5*). However, the interactions with the DC-SIGN and DC-SIGNR Ca^{2+} sites are unusual because they involve an internal, rather than a terminal, sugar. In addition to the interactions of the 3- and 4-OHs, the exocyclic C6 packs against Glu^{366} and the 6-OH forms a water-mediated contact with Asn^{379} (Asp^{367} in DC-SIGN) (Fig. 3, A and B). The two mannose residues that form the α1-6 linked branch drape over the solvent-exposed Phe^{325} and Ser^{372} (Fig. 3, C and D). The phenylalanine side chain fits into the crevice between Man3 and Man4, where it makes van der Waals contacts with the central Man3. Ser^{372}, which packs against Phe^{325}, forms hydrogen bonds with the 3-OH of Man4 and a water-mediated hydrogen bond with the 2-OH of Man3. The 3-OH of Man4 also forms a water-mediated hydrogen bond with the backbone amide of Ser^{374}.

The terminal GlcNAc residues also form a number of contacts with DC-SIGN and DC-SIGNR. On the α1-3 branch, the acetamido carbonyl oxygen of GlcNAc1 bonds to Ser^{363} of DC-SIGNR. This position is a valine in DC-SIGN, which participates in van der Waals interactions with GlcNAc1. The contacts between GlcNAc1 with this position are the only major differences in the interactions of these two proteins with the oligosaccharide. In the DC-SIGN crystals, GlcNAc1 also forms a typical C-type lectin Ca^{2+} coordination and hydrogen bond network at the principal Ca^{2+} site on the partner monomer in the dimer, thereby cross-linking the two monomers (Fig. 3B). On the other branch, GlcNAc5 forms a number of hydrogen bond and van der Waals interactions with the protein, fitting into a shelf created by Asn^{323} and Phe^{325} (Fig. 3, C and D).

The majority of oligosaccharides on gp120 are high mannose structures (*14*) (Fig. 1B). Previous studies have shown that both DC-SIGN and DC-SIGNR interact particularly effectively with such structures (*4*). The binding of different types of N-linked oligosaccharides was compared using quantitative inhibition assays as well as glycoprotein and neoglycolipid blots [see table 2 of supplemental data (*11*)]. The competition data reveal that the GlcNAc-terminated pentasaccharide used in the crystal structures is a ligand for DC-SIGN and DC-SIGNR and has an affinity comparable to a five-mannose structure (Man_5). However, though both proteins bind glycoproteins bearing one or more high mannose oligosaccharides, the blotting data show that neither protein binds to complex oligosaccharides attached to glycoproteins (Fig. 1C). Collectively, these data indicate that DC-SIGN and DC-SIGNR are specific for high-mannose N-linked oligosaccharides.

The selectivity of DC-SIGN and DC-SIGNR for high-mannose structures can be understood from the crystal structures and modeling. The two different Manα1-3[Manα1-6]Man moieties present in a model of Man_9 (Fig. 1B) derived from nuclear magnetic resonance (NMR) measurements (*15*) were superimposed on the equivalent portion of the oligosaccharide complexes. Superimposing the inner trimannose branch point reveals that the core GlcNAc residue linked β1-4 to the first mannose clashes with Phe^{325} (Fig. 4). Modeling reveals steric clashes with the phenylalanine even when the extreme values of the observed torsion angles (*13*) are used. In contrast, superposition of the outer trimannose branch point (Fig. 1B, yellow) reveals no steric clashes of the Man_9 structure with DC-SIGN or DC-SIGNR. Therefore, although these CRDs recognize the trisaccharide Manα1-3[Manα1-6]Man, in the context of N-linked glycans they can only do so when the central mannose is linked in the α anomeric configuration, a structure found only in high-mannose oligosaccharides (compare Fig. 1, B and C). Phe^{325} plays two essential roles: it forms part of the surface complementary to the shape of the Manα1-6Man moiety (Fig. 3, C and D) and it also provides dis-

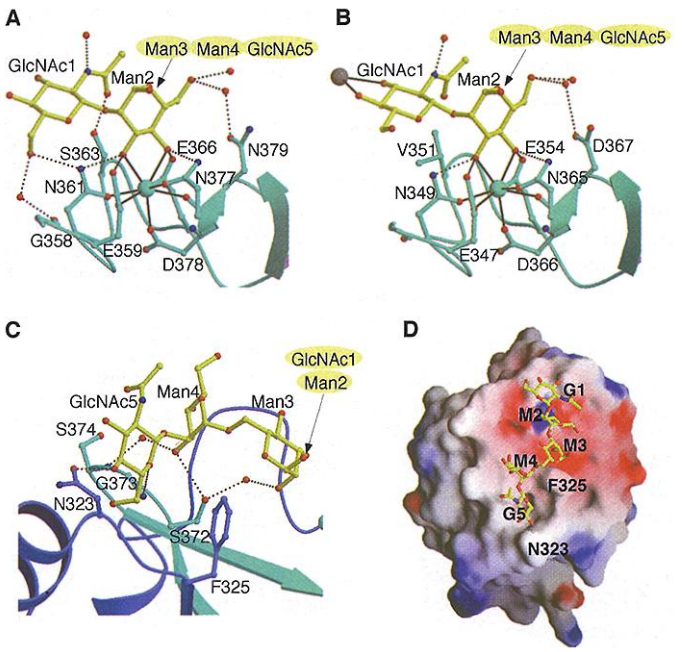

Fig. 3. Interactions of DC-SIGN and DC-SIGNR with $GlcNAc_2$-Man_3. **(A)** Interaction of the α1-3–linked branch with DC-SIGNR. For clarity, the remaining sugar residues are shown schematically. Ca^{2+} coordination bonds are shown as solid black lines; hydrogen bonds, as dashed lines. Large cyan sphere is Ca^{2+}; red, oxygen; blue, nitrogen. **(B)** Interactions of the α1-3–linked branch with DC-SIGN. The terminal GlcNAc1 forms a cross-link by forming the typical C-type lectin interactions with the principal Ca^{2+} site of another CRD. For clarity, only the coordination bonds to the Ca^{2+} (gray) are shown. **(C)** Interaction of the α1-6–linked branch with DC-SIGNR, including the central (reducing) mannose (Man3). Different portions of the protein backbone are shown in two shades of blue. The interaction of this branch with DC-SIGN is essentially the same. **(D)** Electrostatic surface representation of the DC-SIGNR CRD, showing the interaction with the bound oligosaccharide. Asn^{323} and Phe^{325}, which form a shelf that interacts with the Manα1-6Man branch, are indicated. Regions of positive and negative electrostatic potential (10 kT/e level) are shown in blue and red, respectively. (D) was made with GRASP (*19*).

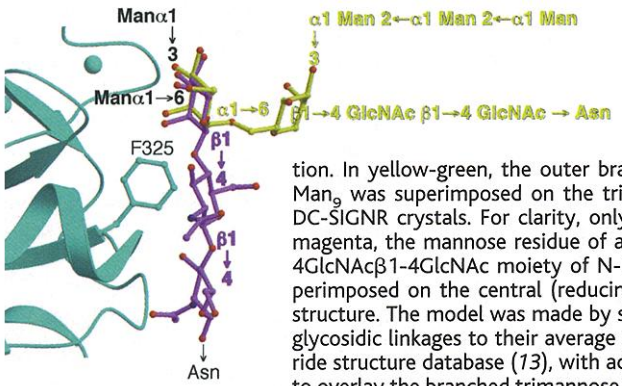

Fig. 4. A phenylalanine prevents binding of the inner trimannosyl core of N-linked oligosaccharides. The DC-SIGNR CRD is shown in cyan, with the Phe^{325} side chain in a ball-and-stick representation. In yellow-green, the outer branched trimannose structure of Man_9 was superimposed on the trimannose structure seen in the DC-SIGNR crystals. For clarity, only the α1-6 branch is shown. In magenta, the mannose residue of a model of the internal Manβ1-4GlcNAcβ1-4GlcNAc moiety of N-linked oligosaccharides was superimposed on the central (reducing) mannose of the trimannose structure. The model was made by setting the torsion angles of the glycosidic linkages to their average values found in an oligosaccharide structure database (*13*), with adjustments in the torsion angles to overlay the branched trimannose structure precisely. The clash of the first GlcNAc with Phe^{325} is evident. In both the positions of the α1-3 and α1-6 linked mannose residues linked to the central mannose of the trimannose structure are indicated in the black text.

crimination between the inner and outer trimannose structures by preventing binding to the inner branch point mannose. Selective binding of DC-SIGN and DC-SIGNR to the outer branched trimannose moiety can explain almost all of their binding characteristics (*16*).

Mannose-binding proteins (MBPs) are C-type lectins that function in innate immunity by recognizing carbohydrate structures characteristic of pathogens, and they do not bind strongly to mannose-type ligands present on host cell surfaces (*5*). Although the CRDs of DC-SIGN and DC-SIGNR share 24% sequence identity with rat serum MBP, the mode of binding of oligosaccharides to MBP is quite distinct from the interaction of DC-SIGN and DC-SIGNR with the branched trimannose structure. Each CRD in MBP interacts with a single terminal mannose or GlcNAc residue in an oligosaccharide ligand, and the rest of the oligosaccharide points away from the surface of the protein (*17*) (Fig. 2B). The architecture of the MBP trimer places the binding sites in the three CRDs far enough apart that MBP binds with high avidity only to the repetitive and dense arrays presented on pathogenic cell surfaces, but not to the more closely spaced terminal mannose residues present on endogenous oligosaccharides (*18*). In contrast, the interactions of DC-SIGN and DC-SIGNR with endogenous glycans on T cells and the HIV envelope result from high affinity binding to a characteristic internal feature of high-mannose oligosaccharides.

DC-SIGN– and DC-SIGNR–gp120 interactions represent a potential target for anti-HIV therapy aimed at disrupting the DC-virus interaction at primary sites of infection, in order to lower the efficiency of T cell infection. Although the high avidity generated by clustering low-affinity lectin monomers into oligomeric structures has made it difficult to design drugs aimed at disrupting protein-carbohydrate interactions, the unusually high affinity between the monomeric DC-SIGN or DC-SIGNR CRDs and high-mannose oligosaccharides (*4*) suggests that they may be useful targets. The mechanistic basis of the DC-SIGN– and DC-SIGNR–oligosaccharide interactions presented here provides a starting point for design of such therapeutics, which would attack the viral infection at a novel stage and which could potentially be prophylactic. Lastly, these studies suggest that the interaction of DC-SIGN and DC-SIGNR with endogenous ligands may not be restricted to ICAMs that have been studied to date, but may include other cell surface or soluble glycoproteins with appropriately displayed high mannose oligosaccharides.

References and Notes

1. J. Banchereau, R. M. Steinman, *Nature* **392**, 245 (1998).
2. T. B. H. Geijtenbeek *et al.*, *Cell* **100**, 575 (2000).
3. T. B. H. Geijtenbeek *et al.*, *Nature Immunol.* **1**, 353 (2000).
4. D. A. Mitchell, A. J. Fadden, K. Drickamer, *J. Biol. Chem.* **276**, 28939 (2001).
5. W. I. Weis, M. E. Taylor, K. Drickamer, *Immunol. Rev.* **163**, 19 (1998).
6. E. J. Soilleux, R. Barten, J. Trowsdale, *J. Immunol.* **165**, 2937 (2000).
7. S. Pöhlmann *et al.*, *Proc. Natl. Acad. Sci. U.S.A.* **98**, 2670 (2001).
8. A. A. Bashirova *et al.*, *J. Exp. Med.* **193**, 671 (2001).
9. T. B. H. Geijtenbeek *et al.*, *Cell* **100**, 587 (2000).
10. S. Pöhlmann *et al.*, *J. Virol.* **75**, 4664 (2001).
11. Supplemental data are available on *Science* Online at www.sciencemag.org/cgi/content/full/294/5549/2163/DC1.
12. K. Drickamer, *Curr. Opin. Struct. Biol.* **9**, 585 (1999).
13. A. J. Petrescu, S. M. Petrescu, R. A. Dwek, M. R. Wormald, *Glycobiology* **9**, 343 (1999).
14. T. Mizuochi *et al.*, *J. Biol. Chem.* **265**, 8519 (1990).
15. R. J. Woods, A. Pathiaseril, M. R. Wormald, C. J. Edge, R. A. Dwek, *Eur. J. Biochem.* **258**, 372 (1998).
16. The weak interaction with a GlcNAc-terminated neoglycolipid derived from an asialo, aglacto-bantennary N-linked glycan can be explained by the interaction of a terminal GlcNAc residue with the principal Ca^{2+} site, as observed in the cross-linked pairs of CRDs of DC-SIGN (Fig. 3B). This interpretation is confirmed by the observation that the corresponding galactose-terminated structure, in which the 4-OH of GlcNAc is inaccessible, does not bind at all. Moreover, modeling of a further mannose residue in α1-2 linkage to the Manα1-3Man arm of the trimannosyl moiety suggests that it would pack against Val^{351} of DC-SIGN, whereas no contact would be made with the smaller Ser^{363} present at this position of DC-SIGNR. This observation may be related to the larger affinity difference between Man_9 and smaller oligosaccharides displayed by DC-SIGN relative to DC-SIGNR [see (*4*) and table 2 of supplemental data (*11*)].
17. W. I. Weis, K. Drickamer, W. A. Hendrickson, *Nature* **360**, 127 (1992).
18. W. I. Weis, K. Drickamer, *Structure* **2**, 1227 (1994).
19. A. Nicholls, GRASP: Graphical Representation and Analysis of Surface Properties (Columbia University, New York, 1992).
20. Z. Otwinowski, W. Minor, *Methods Enzymol.* **276**, 307 (1997).
21. R. A. Laskowski, M. W. MacArthur, D. S. Moss, J. M. Thornton, *J. Appl. Crystallogr.* **26**, 283 (1993).

22. We thank E. Soilleux for providing cDNAs; D. Torgersen for assistance with protein preparation; G. Golan, O. Livnah, and G. Shoham of the Hebrew University for assistance with data collection; and L. Tong for the COMO program. Some of this work is based upon research conducted at the Stanford Synchrotron Radiation Laboratory (SSRL), a national facility operated by Stanford University for the DOE, Office of Basic Energy Sciences. The SSRL Structural Molecular Biology Program is supported by the Department of Energy, Office of Biological and Environmental Research and by the National Center for Research Resources, Biomedical Technology Program and National Institute of General Medical Sciences, NIH. Part of this research was carried out at the National Synchrotron Light Source, Brookhaven National Laboratory, which is supported by the DOE, Division of Materials Sciences and Division of Chemical Sciences. Supported by grants 041845 and 054508 from the Wellcome Trust (K.D.), and grant GM50565 from the NIH (W.I.W.). Coordinates and structure factors have been deposited in the Protein Data Bank, with accession codes 1K9I (DC-SIGN) and 1K9J (DC-SIGNR).

19 September 2001; accepted 1 November 2001

A Transgenic Model of Visceral Obesity and the Metabolic Syndrome

Hiroaki Masuzaki,[1] Janice Paterson,[2,3] Hiroshi Shinyama,[1] Nicholas M. Morton,[2] John J. Mullins,[3] Jonathan R. Seckl,[2] Jeffrey S. Flier[1]*

The adverse metabolic consequences of obesity are best predicted by the quantity of visceral fat. Excess glucocorticoids produce visceral obesity and diabetes, but circulating glucocorticoid levels are normal in typical obesity. Glucocorticoids can be produced locally from inactive 11-keto forms through the enzyme 11β hydroxysteroid dehydrogenase type 1 (11β HSD-1). We created transgenic mice overexpressing 11β HSD-1 selectively in adipose tissue to an extent similar to that found in adipose tissue from obese humans. These mice had increased adipose levels of corticosterone and developed visceral obesity that was exaggerated by a high-fat diet. The mice also exhibited pronounced insulin-resistant diabetes, hyperlipidemia, and, surprisingly, hyperphagia despite hyperleptinemia. Increased adipocyte 11β HSD-1 activity may be a common molecular etiology for visceral obesity and the metabolic syndrome.

Obesity is associated with adverse metabolic consequences such as diabetes and dyslipidemia (*1*). The best predictor of these morbidities is not the total body adipose mass, but the specific quantity of visceral fat (*2*, *3*). A molecular basis for disproportionate accumulation of visceral fat has not been identified and the extent to which visceral adiposity causes or merely reflects the associated metabolic syndrome, which includes insulin resistance, glucose intolerance, and dyslipidemia, remains unclear (*3*).

One identified cause of visceral obesity and metabolic complications is exposure to